Copy 5
RM L57H07

NACA RM L57H07

NACA

RESEARCH MEMORANDUM

[redacted]

A NOTE ON THE ABILITY TO PREDICT TRANSONIC DRAG-RISE CHANGES DUE TO MODEL MODIFICATIONS

By P. Kenneth Pierpont

Langley Aeronautical Laboratory
Langley Field, Va.

NATIONAL ADVISORY COMMITTEE FOR AERONAUTICS

WASHINGTON

October 3, 1957

[redacted]

NATIONAL ADVISORY COMMITTEE FOR AERONAUTICS

RESEARCH MEMORANDUM

A NOTE ON THE ABILITY TO PREDICT TRANSONIC DRAG-RISE CHANGES DUE TO MODEL MODIFICATIONS

By P. Kenneth Pierpont

SUMMARY

An experimental and analytical study was made at transonic speeds up to a Mach number of 1.43 to ascertain the ability of present calculation procedures to predict transonic drag-rise changes which result from physical model changes. The experimental data were obtained in the Langley 8-foot transonic tunnel and the Langley 8-foot transonic pressure tunnel at Reynolds numbers based on the mean aerodynamic chord near 2×10^6. Both wing-body and wing-body-tail configurations were investigated.

The results showed that, with the exception of a model having a relatively bluff forebody and afterbody, the use of current techniques utilizing a Fourier analysis to fit the area slope curve of the equivalent body provided estimates of transonic drag within 15 percent of the measured values for wing-body-tail configurations. When a well-shaped configuration was chosen as a basis, present calculative procedures permitted estimates of the change in drag rise which resulted from physical change in the model which were considered accurate enough to be useful for preliminary design.

INTRODUCTION

The application of the transonic and supersonic area rules (refs. 1 and 2) aroused considerable interest in methods for numerically estimating transonic and supersonic wave drags. Computing techniques such as those outlined in references 3 and 4 have been effectively used for estimating the zero-lift drag-rise coefficients at transonic speeds of model configurations (refs. 5 and 6, for example) and for complete configurations in reference 7.

The ability to predict transonic drag-rise coefficients above $M = 1.02$ closer than the 20-percent value stated in reference 3 depends in part at least upon the experience of the computer and the characteristics of the

[redacted]

individual configuration. For those cases in which performance estimates demand more accurate information, resort to wind-tunnel or free-flight model tests becomes a necessity. However, since a given basic configuration may change considerably as the design progresses, some method for estimating the effects of external modifications is needed. The purpose of the present study was to determine if the changes in drag rise associated with physical modifications can be adequately predicted by the numerical procedures presently available.

A swept wing and tail model, typical of current fighter designs, was tested in the Langley 8-foot transonic tunnel and in the Langley 8-foot transonic pressure tunnel. Various arrangements of fuselage modifications together with wings and tails of different thicknesses were employed. The Mach number range extended from subcritical speeds to 1.2 and in some cases to 1.4, and the Reynolds number based on the wing mean aerodynamic chord was about 2×10^6.

SYMBOLS

A	cross-sectional area, normal to free-stream direction
A_n	Fourier coefficient of nth term
C_D	drag coefficient, Drag/qS
ΔC_D	drag-rise coefficient, $\left(C_D - C_{D,M=0.8}\right)$
$\Delta C_D'$	incremental drag-rise coefficient, corresponding to drag rise of an equivalent body having an area distribution for a particular Mach number at a particular value of ϕ
l	body length
M	Mach number
N	number of terms used in Fourier sine series
q	dynamic pressure
S	wing area
x	distance along X-axis, measured from body nose

ϕ angle between Z-axis and line in YZ-plane normal to intersection of cutting plane with YZ-plane (see fig. 1)

θ longitudinal position angle, $\cos^{-1}\left(1 - \frac{2x}{l}\right)$

MODEL AND TESTS

The model consisted of a nonaxisymmetric fuselage having the wing mounted on top with 42° of quarter-chord sweepback and an aspect ratio of 3.4. Model details are shown in figure 2 and table I. Tail surfaces, when used, had 45° quarter-chord sweep and aspect ratios of 2.0 and 1.5 for the horizontal and vertical tails, respectively.

Two wings, made up of straight-line elements, were employed; the one having a taper in thickness from 6 to 5 percent was called the basic wing and the other of a uniform 4-percent thickness was called the thin wing. Similarly two sets of tail surfaces were used, the basic tails having a taper in thickness from 6 to 4 percent and the thin tails having a uniform 4-percent thickness. Symmetrical airfoil sections of the NACA 65A series were used for all surfaces.

Several fuselage configurations, designated by letters, are shown in figure 3. A configuration described by letter only signifies a basic wing and body; whereas, a letter with a prime signifies a body with basic wing and tails, and the subscript 1 with either the letter or the letter and prime indicates that the 4-percent-thick surfaces have been installed in place of the tapered-in-thickness surfaces. For example: C designates body C with basic wing, C' designates body C with basic wing and basic tails, and C'_1 designates body C with thin wing and thin tails.

The experimental investigation was conducted in both the Langley 8-foot transonic and the Langley 8-foot transonic pressure tunnels described in references 8 and 9. A sketch of the model in the Langley 8-foot transonic pressure tunnel is shown in figure 4. Mach numbers extended from 0.8 to about 1.2 with a few points being obtained at 1.43. Reynolds number based on the wing mean aerodynamic chord was about 2.0×10^6.

Zero-lift drag was obtained from faired polars for a small range of angles near zero lift. Estimated accuracy for the drag-coefficient data is considered to be about ±0.001. Although there is some difference in the turbulence characteristics of the two tunnels, unpublished data indicate that the difference in zero-lift drag coefficient measured in both tunnels is approximately constant throughout the range of test Mach numbers. Comparisons of drag-rise coefficients obtained in either facility should therefore be valid.

COMPUTATIONS

The computations necessary to obtain the drag-rise coefficients were carried out in the manner outlined in reference 3. The drag-rise coefficient for a complete configuration was defined as

$$\Delta C_D = \frac{1}{2\pi} \int_0^{2\pi} \Delta C_D' \, d\phi \tag{1}$$

in which $\Delta C_D'$ is termed the incremental drag-rise coefficient and is the calculated drag-rise coefficient for the equivalent body corresponding to a particular single area distribution at the angle ϕ. (See fig. 1.) Accordingly, from reference 3,

$$\Delta C_D' = \frac{\pi}{4S} \sum_{n=1}^{N} n A_n^2 \tag{2}$$

Values of A_n were obtained by conventional Fourier analysis techniques on a digital computer and are defined as

$$A_n = \frac{2}{\pi} \int_0^{\pi} \frac{dA}{dx} \sin n\theta \, d\theta \tag{3}$$

The wing and tail empennage area distributions were obtained by graphical means. This method was found to be both time consuming and subject to appreciable human inaccuracies. Exploration of numerical methods for obtaining these areas led to solutions which were basically similar to those in references 10 and 11. Check computations by the numerical methods indicated that satisfactory results could readily be obtained and therefore served as a useful check on the graphical solutions.

Area distributions normal to the longitudinal axis of the fuselage were obtained by integrating photographically reproduced cross sections cut from plaster of Paris mold patterns. In the region of the wing-body juncture as well as in the region of the tail-body junctures a small portion of the surface was arbitrarily included in the defined fuselage area to simplify the work.

Total equivalent-body area distributions were obtained by combining the various components as outlined in reference 12. In this reference, it was suggested that the cross-sectional area for the wing or horizontal tail be combined with the fuselage areas at the longitudinal stations where the oblique cutting planes for the wing or tail cross the plane of lateral symmetry. Cross-sectional areas for the vertical tail were combined with the fuselage areas at the stations where the cutting planes crossed the upper surface of the fuselage near the base of the tail.

Slopes of the area distributions were derived numerically by using a five-point analysis for 120 points equally spaced along the body length. A check on the validity of the slope curves was obtained by plotting and integrating mechanically to insure the proper closed body. Thirty-three harmonics were computed for all configurations after it had been noted that the area distribution was not adequately represented by the initially selected 24 harmonics.

RESULTS AND DISCUSSION

The availability of data for several body configurations tested in conjunction with different wing and tail thicknesses has enabled an evaluation of available methods for computing the drag-rise-coefficient changes which resulted from diverse model modifications. For convenience of presentation, the results have been arranged in two categories. The first group, figures 5 and 6, consists of wing-body configurations and includes some of the effects of wing thickness. The second group, figures 7 and 8, consists of wing-body-tail configurations and includes additional effects of wing and tail thickness. Representative variation of the incremental drag-rise coefficient, which is the drag rise for a body having the area distribution equivalent to that for a particular cutting-plane angle ϕ, with the cutting-plane angle is shown on figure 9. The tapered-in-thickness wing and tail will hereinafter be referred to as the basic wing and tails and the uniform thickness 4-percent wing and tails will be termed the thin wing and tails.

Wing-Body Configurations

Body shape.- Longitudinal equivalent-body area distributions for three wing-body configurations with the basic wing and two wing-body configurations with the thin wing are shown in figure 5 for three principal cutting planes. Model A is shown to have a blunt forebody shape and a large negative slope near the base. The representative area slope-distribution curve shown in figure 6 illustrates this more readily. Substantial reductions in local slopes at both nose and tail were achieved

by lengthening and slenderizing the forebody and by adding a small extension to the model base; these changes are illustrated by body B (see also fig. 3).

Further improvement in the overall area distribution was achieved by filling in the hollow ahead and behind the maximum area of body B to obtain model C. These area additions were obtained from an approximate average area distribution for $M = 1.2$ by using a tangent straight line across the hollow as described in reference 11. The area to be added was then divided so that approximately one-half was added above and one-half below the wing chord plane. The representative slope-distribution curves of figure 6 show that this modification has reduced the magnitude of the peak slopes. Also shown in the figure are a number of check points used to establish the degree of approximation for body B obtained from the Fourier analysis. These check points are representative of the agreement achieved throughout the analysis.

Comparisons of calculated and experimental drag-rise coefficients are shown in figure 10(a). It appears plausible that the lack of agreement for model A could be attributed to the inability of the theory to properly account for the relatively bluff forward and rearward portions of the body. The agreement between calculated and experimental results for models B and C are excellent. The estimated change in drag-rise coefficient between models B and C agreed within about 30 percent with the measured values at both $M = 1.0$ and 1.2.

Wing thickness.- The two models, B_1 and F_1, in figure 5 were equipped with the thin wing of 4-percent thickness. Body F was nearly identical to body C. Principal effect of reducing the wing thickness on the equivalent-body geometry was to increase the equivalent-body fineness ratio which can be seen from figure 5. Because body F had been designed with the basic wing, some overfilling of the hollows ahead and behind the maximum area is evident when used with the thin wing, especially at $\phi = 0^\circ$ and 90°. For these configurations only the calculated drag-rise coefficients were obtained. Values of $C_D = 0.0146$ and 0.0133 correspond to configuration B_1 and F_1, respectively, for $M = 1.2$. Compared to configuration B, the change in drag-rise coefficient resulting from the wing modification (model B_1) would be 0.0071 and compared to C the change resulting from the wing modification (model F_1) would be only 0.0024.

Wing-Body-Tail Configurations

Body shape.- Longitudinal equivalent-body area distributions for five wing-body-tail configurations using the basic wings and tails are shown in figure 7. Two configurations for which the thin wings and tails

were employed are compared in figure 8. In the latter figure, body F was nearly identical to body C.

Comparison of the calculated values of incremental drag coefficient as a function of circumferential position angle or cutting plane angle are shown in figure 9 for configurations A', B', and C'. Variation with ϕ is appreciably different for the three models. Model C especially bears little resemblance to either of the others. Different variations with ϕ such as are shown were typical of many of the configurations. Caution should therefore be exercised when attempting to predict overall drag-rise changes on the basis of area distributions for a single cutting-plane angle.

Experimental drag-rise coefficients have been compared with the corresponding calculated values in figure 10(b) for both $M = 1.2$ and 1.37. As was the case for the wing-body configuration alone, model A' is shown to be overestimated by a significant amount. The calculations were in substantial agreement with the test data for models B', C', D', and E'. Model D' was obtained by deliberately overfilling the area distribution to obtain a shape, based on the average area curve, approximating an ideal-slender-body-theory shape as outlined in reference 11 near the maximum area. Model E was obtained by first indenting the fuselage underneath the wing only in the region of the maximum area by about 10 percent of the equivalent-body maximum area, an amount considered a maximum without interfering with an engine, and then filling in the remaining depression in the area distribution curve in a manner similar to that for configuration C'. Inconsequential improvement for model E' as compared to model C' was measured and the calculations actually showed a small drag increase. The calculated drag rise for model E' was the only actual inconsistency in the calculations and is not surprising since the theory cannot be expected to account for very small drag reducing changes in configurations. A similar case of asymmetric indentation was shown to have an adverse effect on the drag rise for a delta wing in reference 13. The decrease in friction drag with Mach number, however, would tend to improve the agreement between computed and experimental results particularly at the higher Mach number ($M = 1.37$).

The effects of body-shape change on the calculated drag rise with the thin wings and tails (fig. 8) are shown in figure 10(c) compared to that for model B'. For configurations B'_1 and F'_1, the body shapes were the same as those previously used with the thick wings and tails. These shapes, therefore, do not necessarily represent near-optimum shapes but still are useful for comparison. Figure 10(c) indicates that the calculated and measured values are in fair agreement for model B'_1 and in good agreement for model F'_1. Furthermore, the improvement which would be predicted did not materialize.

For the design of an actual airplane, total drag instead of drag rise is the important parameter. For the present wing-body-tail configurations, an average subcritical drag coefficient was found to be 0.015. By using this value together with the calculated drag-rise coefficient, the error in estimated transonic drag was less than 15 percent except when body A was utilized.

Wing and tail thickness.- Generally, the effect of reducing the wing and tail thicknesses was to reduce the component drag-rise contributions and to increase the overall fineness ratio of the equivalent body. Comparison of figure 10(c) shows that, for body B, the reduction in wing and tail thickness resulted in drag-coefficient decreases which were adequately predicted to be about 0.010. Comparing model C' and F'_1 for which bodies C and F were nearly identical, shows that the calculated drag-rise coefficients agreed well with the measured values. The change in drag coefficient due to thickness change was only about one-half as much for body F as with body B, or about 0.005. This comparison therefore indicates that the improved body shape had eliminated much of the interference drag and that the remaining change was largely a result of the wing and tail wave drag.

Drag-Rise Change

The results have generally shown that the calculated and experimental results are in better agreement for those models having improved area distributions. The results have been replotted in figure 11 in the form of drag-rise changes. Drag-rise change is defined as the increase or decrease in drag rise resulting from a configuration change whether measured or calculated. For example, the drag-rise change for model C' referred to the base of B' is $\left|C_{D,B'} - C_{D,C'}\right|$. Both the tail-off and tail-on configurations have been compared on the basis of model B, whereas tail-on configurations have been compared on the basis of model B'. The amount of overestimation or underestimation resulting from the calculations is shown by appropriate shading, and, except for the model with body A, the method is considered accurate enough to be useful for preliminary engineering design studies.

CONCLUSIONS

An experimental and analytical study has been made in the Langley 8-foot transonic tunnel and in the Langley 8-foot transonic pressure tunnel to ascertain the ability of present calculation techniques to predict transonic drag-rise changes. The following conclusions are believed applicable:

1. With the exception of a model having a relatively bluff forebody and afterbody, the use of currently available calculative procedures provided estimates of transonic drag for wing-body-tail configurations within 15 percent of the measured values.

2. When a well-shaped configuration was chosen at the outset, present calculative procedures permitted predictions of the change in drag rise, resulting from physical change in the model, which are considered accurate enough to be useful for preliminary design.

Langley Aeronautical Laboratory,
National Advisory Committee for Aeronautics,
Langley Field, Va., July 18, 1957.

REFERENCES

1. Whitcomb, Richard T.: A Study of the Zero-Lift Drag-Rise Characteristics of Wing-Body Combinations Near the Speed of Sound. NACA Rep. 1273, 1956. (Supersedes NACA RM L52H08.)

2. Whitcomb, Richard T., and Fischetti, Thomas L.: Development of a Supersonic Area Rule and an Application to the Design of a Wing-Body Combination Having High Lift-to-Drag Ratios. NACA RM L53H31a, 1953.

3. Holdaway, George H.: Comparison of Theoretical and Experimental Zero-Lift Drag-Rise Characteristics of Wing-Body-Tail Combinations Near the Speed of Sound. NACA RM A53H17, 1953.

4. Holdaway, George H., and Mersman, William A.: Application of Tchebichef Form of Harmonic Analysis to the Calculation of Zero-Lift Wave Drag of Wing-Body-Tail Combinations. NACA RM A55J28, 1956.

5. Holdaway, George H.: Additional Comparisons Between Computed and Measured Transonic Drag-Rise Coefficients at Zero Lift for Wing-Body-Tail Configurations. NACA RM A55F06, 1955.

6. Loving, Donald L.: A Transonic Investigation of Changing Indentation Design Mach Number on the Aerodynamic Characteristics of a 45° Sweptback-Wing—Body Combination Designed for High Performance. NACA RM L55J07, 1956.

7. Petersen, Robert B.: Comparison of Experimental and Theoretical Zero-Lift Wave-Drag Results for Various Wing-Body-Tail Combinations at Mach Numbers Up to 1.9. NACA RM A56I07, 1957.

8. Wright, Ray H., and Ritchie, Virgil S.: Characteristics of a Transonic Test Section With Various Slot Shapes in the Langley 8-Foot High-Speed Tunnel. NACA RM L51H10, 1951.

9. Matthews, Clarence W.: An Investigation of the Adaptation of a Transonic Slotted Tunnel to Supersonic Operation by Enclosing the Slots With Fairings. NACA RM L55H15, 1955.

10. Jarmolow, K., and Vandrey, F.: An Exact Method for the Rapid Calculation of the Area Distributions of Wings of Trapezoidal Geometry Based on a New Interpretation of the Area Rule. Eng. Rep. No. 7689, The Glenn L. Martin Co., Aug. 24, 1955.

11. Holdaway, George H., and Hatfield, Elaine W.: Investigation of Symmetrical Body Indentations Designed To Reduce the Transonic Zero-Lift Wave Drag of a 45° Swept Wing With an NACA 64A006 Section and With a Thickened Leading-Edge Section. NACA RM A56K26, 1957.

12. Whitcomb, Richart T.: Some Considerations Regarding the Application of the Supersonic Area Rule to the Design of Airplane Fuselages. NACA RM L56E23a, 1956.

13. Hall, James Rudyard: Two Experiments on Applications of the Transonic Area Rule to Asymmetric Configurations. NACA RM L56A25, 1956.

TABLE I.- MODEL DETAILS

Wings:	
Sweepback, quarter-chord, deg	42
Taper ratio	0.25
Aspect ratio	3.4
Mean aerodynamic chord, in.	5.95
Incidence at root, deg	-1
Twist, deg	0
Airfoil sections:	
Basic root	NACA 65A006
Basic tip	NACA 65A005
Thin root	NACA 65A004
Thin tip	NACA 65A004
Horizontal tails:	
Sweepback, quarter-chord, deg	45
Taper ratio	0.15
Aspect ratio, based on total area	1.97
Airfoil sections:	
Basic root	NACA 65A006
Basic tip	NACA 65A004
Thin root	NACA 65A004
Thin tip	NACA 65A004
Vertical tails:	
Sweepback, quarter-chord, deg	45
Taper ratio	0.26
Aspect ratio	1.47
Airfoil sections:	
Basic root	NACA 65A006
Basic tip	NACA 65A004
Thin root	NACA 65A004
Thin tip	NACA 65A004
Fuselages:	
Length (without fairing) of configuration A, in.	25.30
Length of configuration B, in.	27.88
Fineness ratio of configuration A	8.63
Fineness ratio of configuration B	9.45

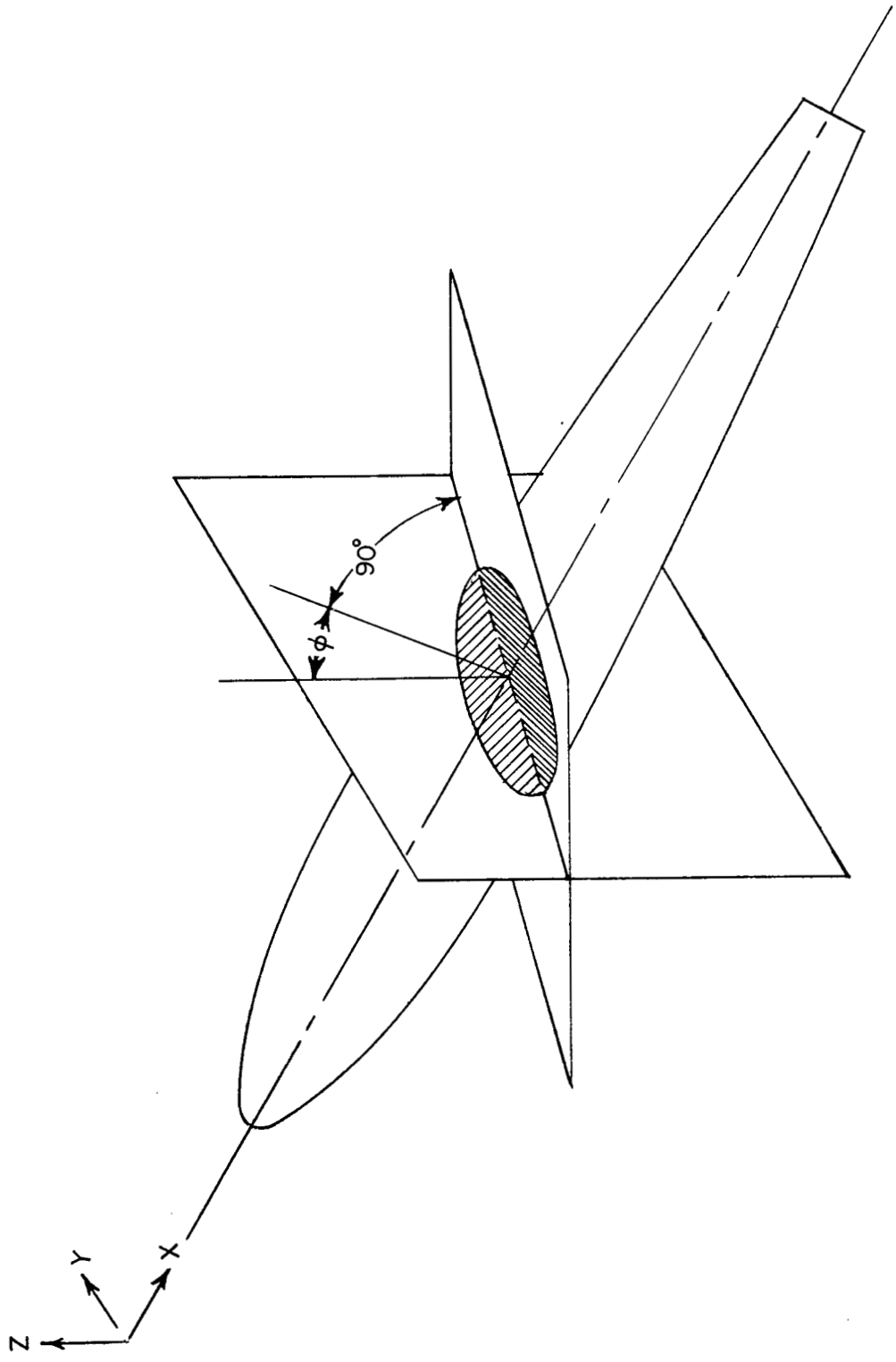

Figure 1.- Sketch of body with reference axes and a typical cutting plane.

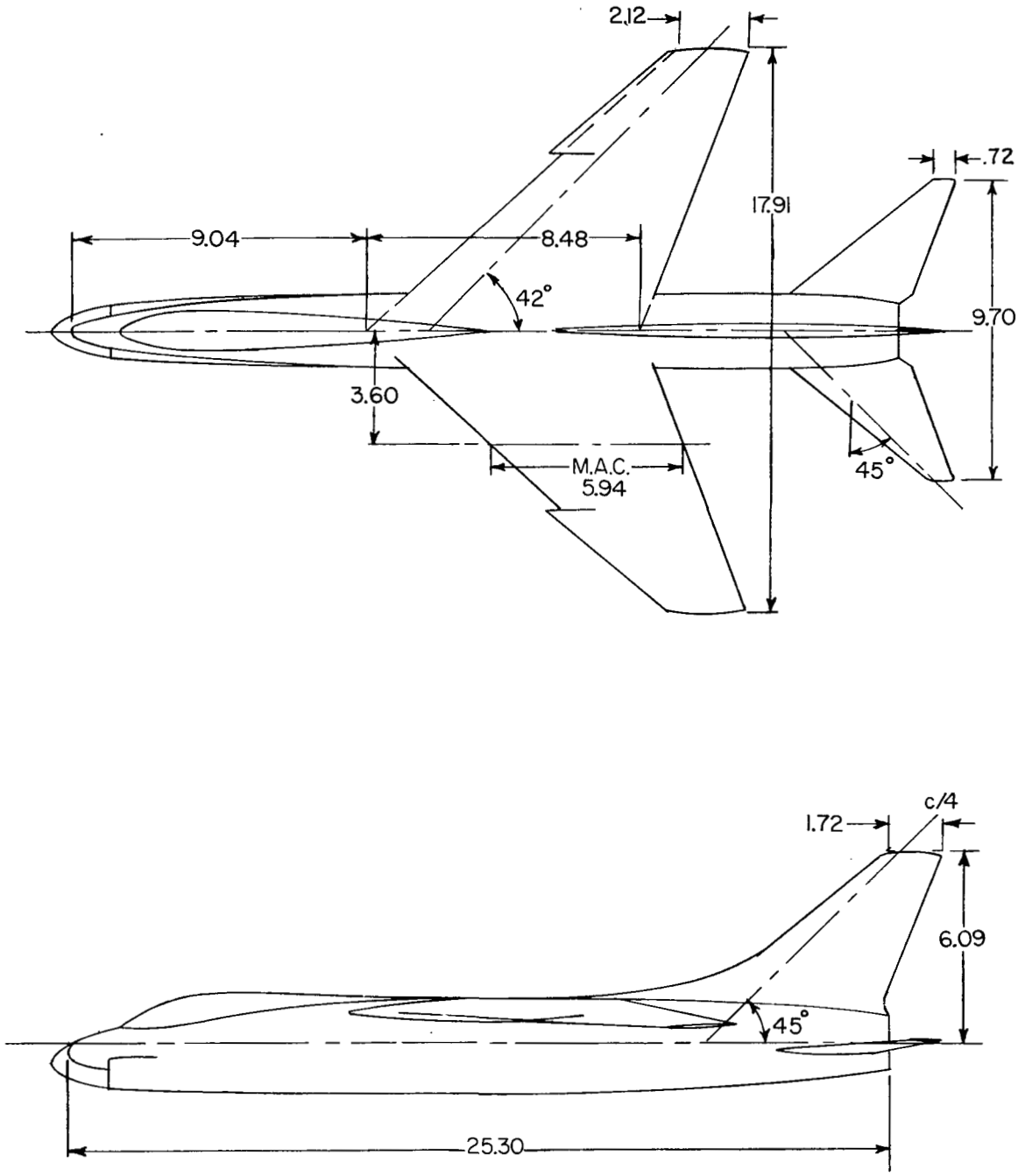

Figure 2.- Principal dimensions of wind-tunnel model. Configuration A'; $\frac{1}{24}$-scale model. (All dimensions are in inches.)

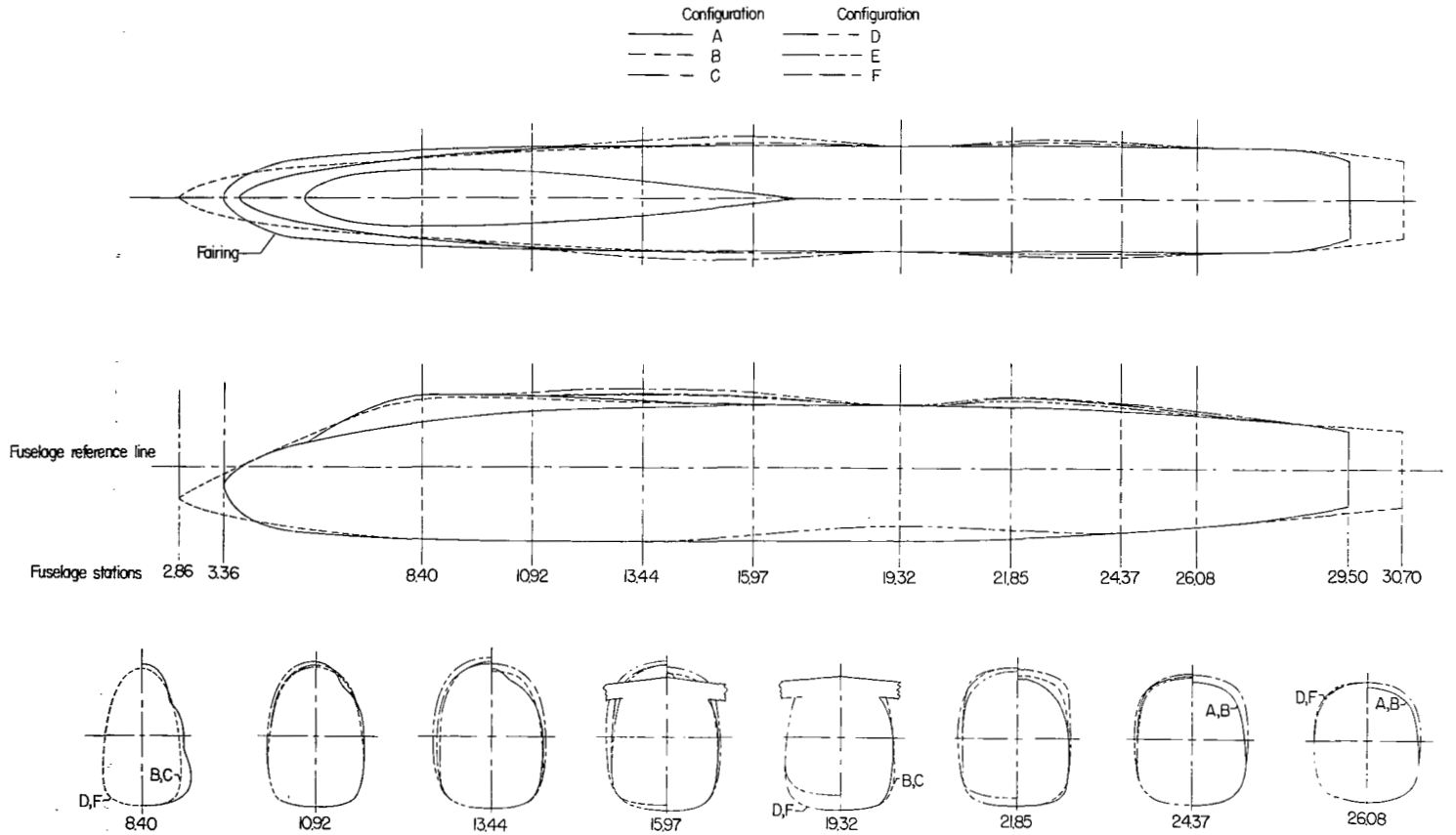

Figure 3.- Line drawings of the area-rule modifications. (All dimensions are in inches for $\frac{1}{24}$-scale model.)

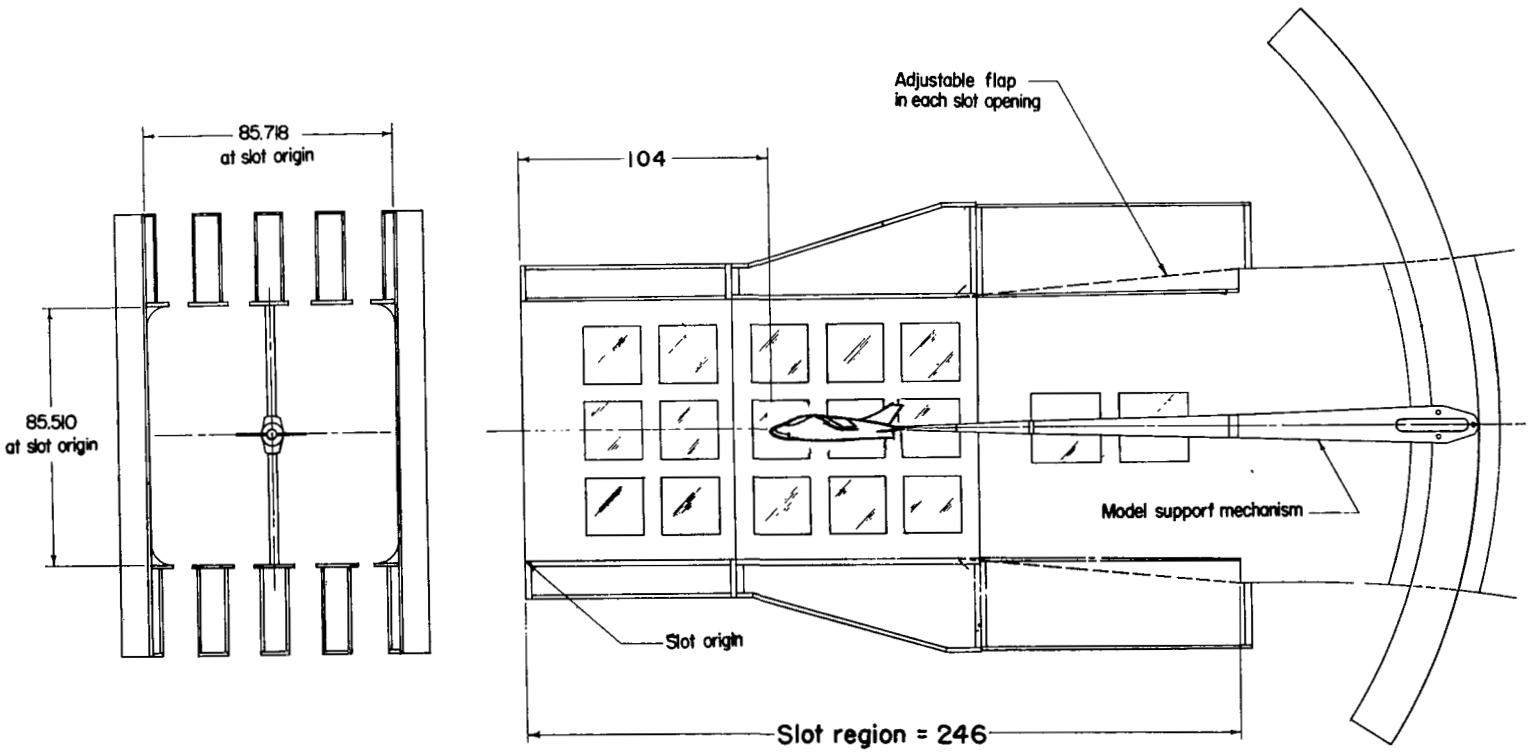

Figure 4.- Sketch of model in Langley 8-foot transonic pressure tunnel. (All dimensions are in inches.)

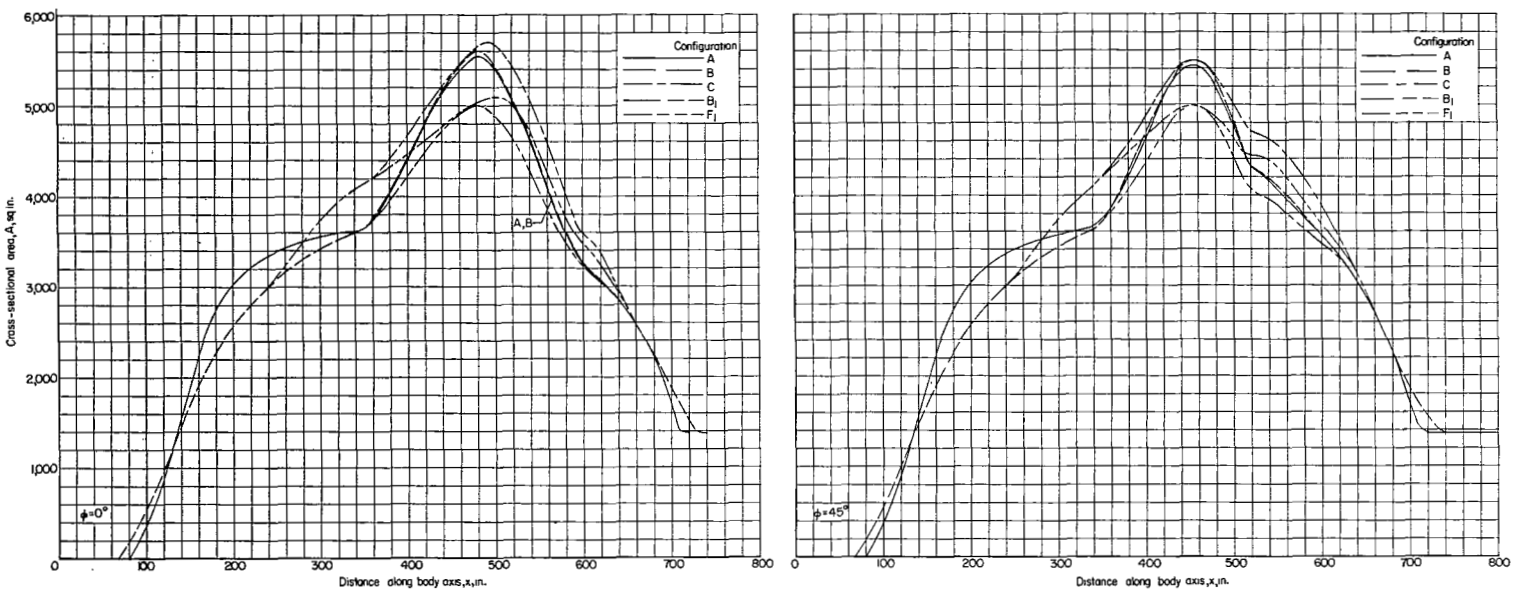

Figure 5.- Comparison of the total-area distributions for the wing-body combination. M = 1.2. (All dimensions are full scale.)

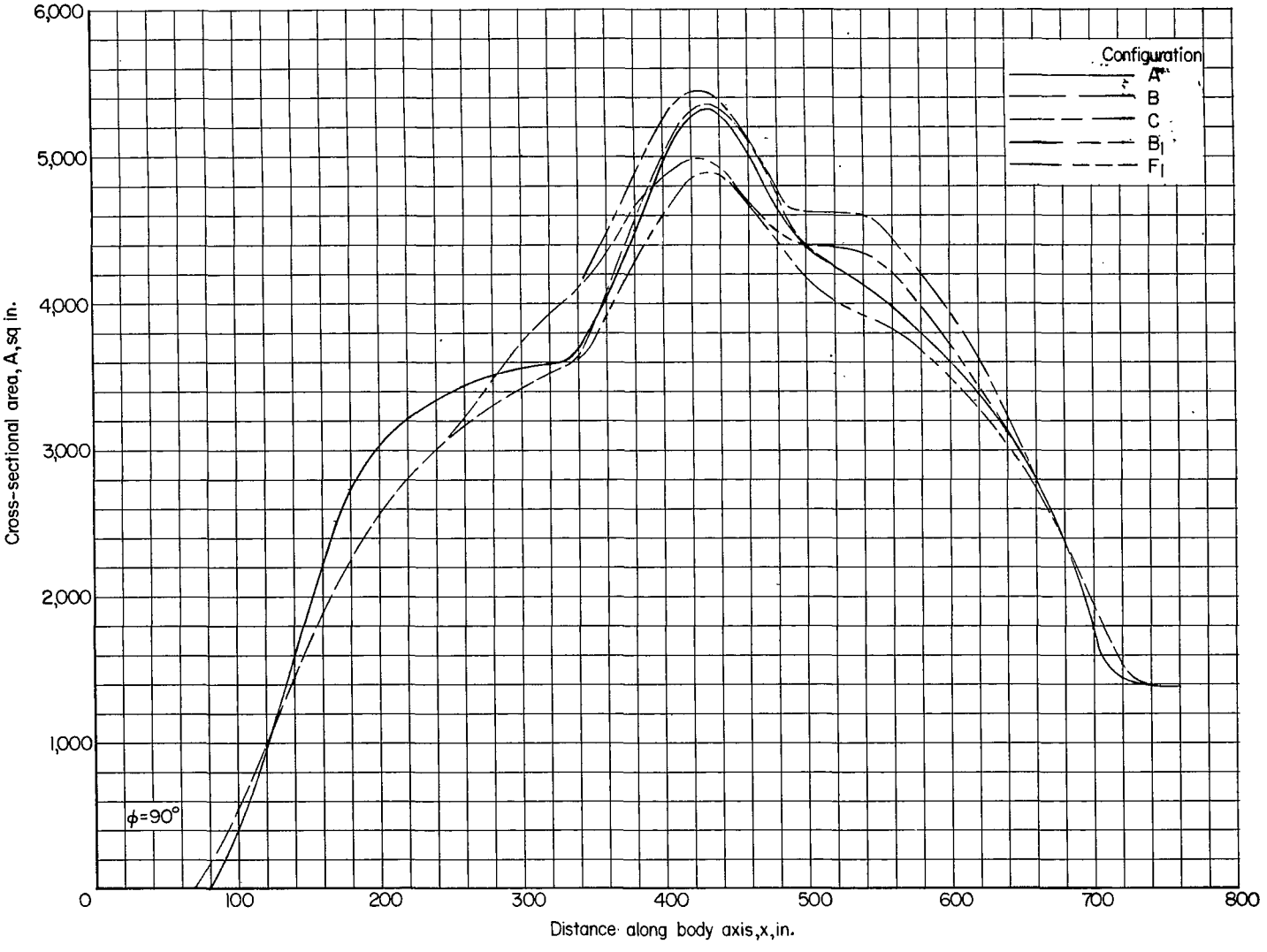

Figure 5.- Concluded.

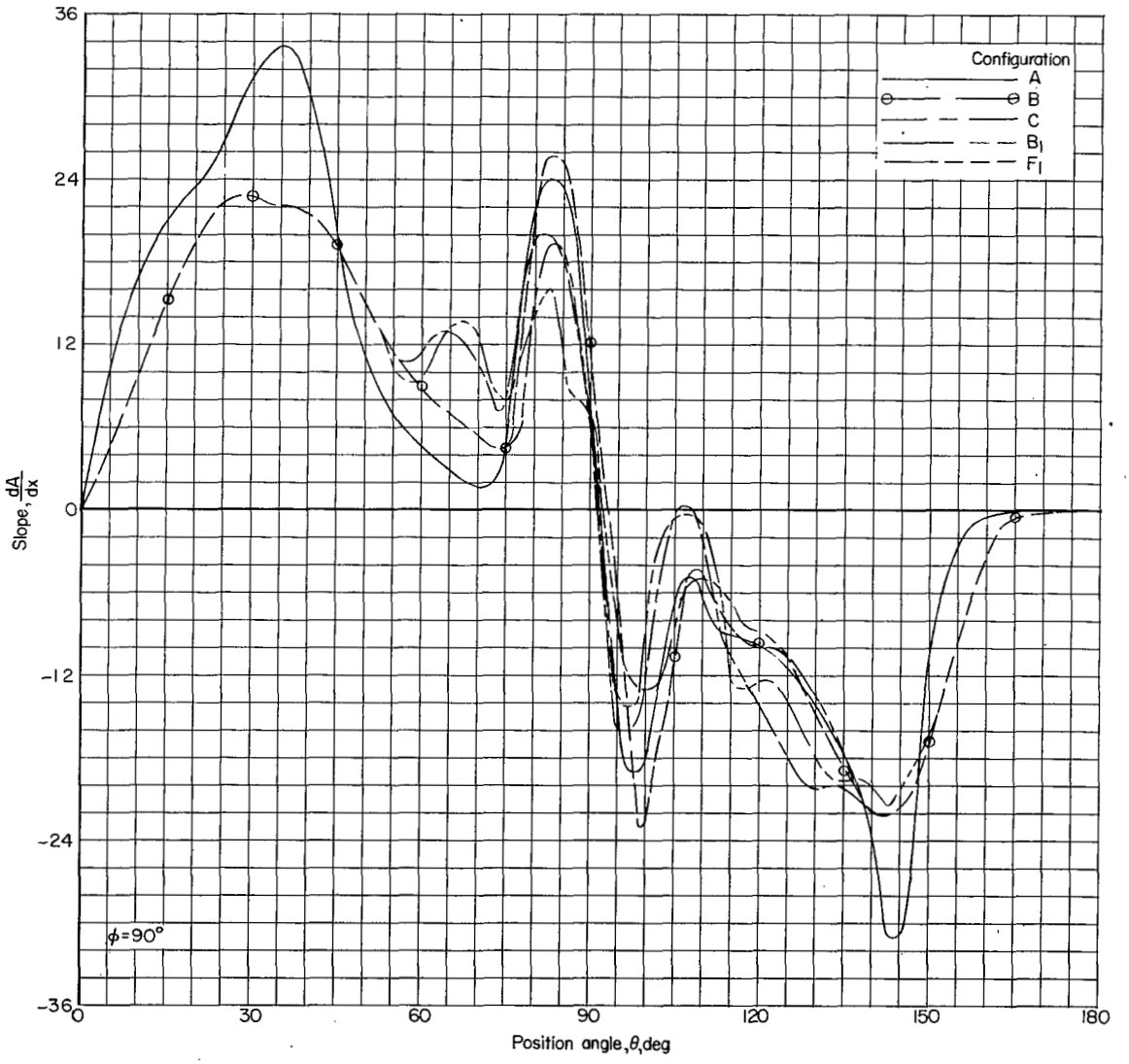

Figure 6.- Comparisons of typical area-slope distributions for the wing-body combination.

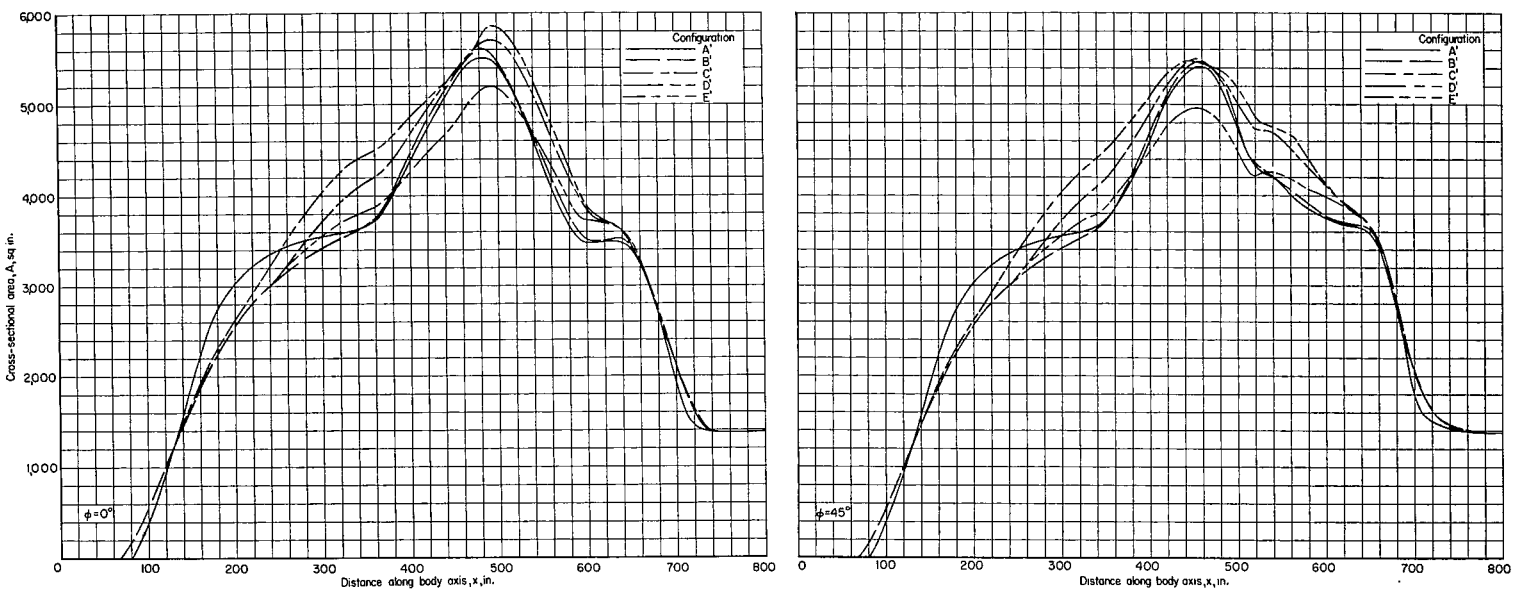

Figure 7.- Comparison of the total-area distributions for the complete model. M = 1.2.
(All dimensions are full scale.)

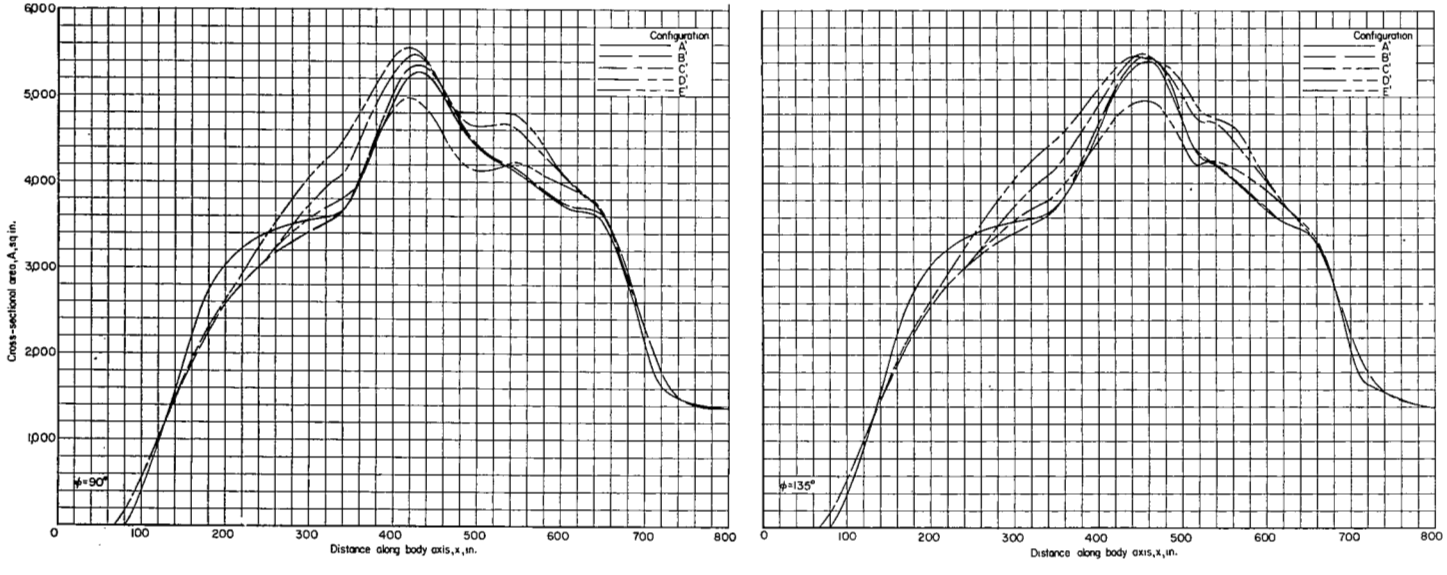

Figure 7.- Continued.

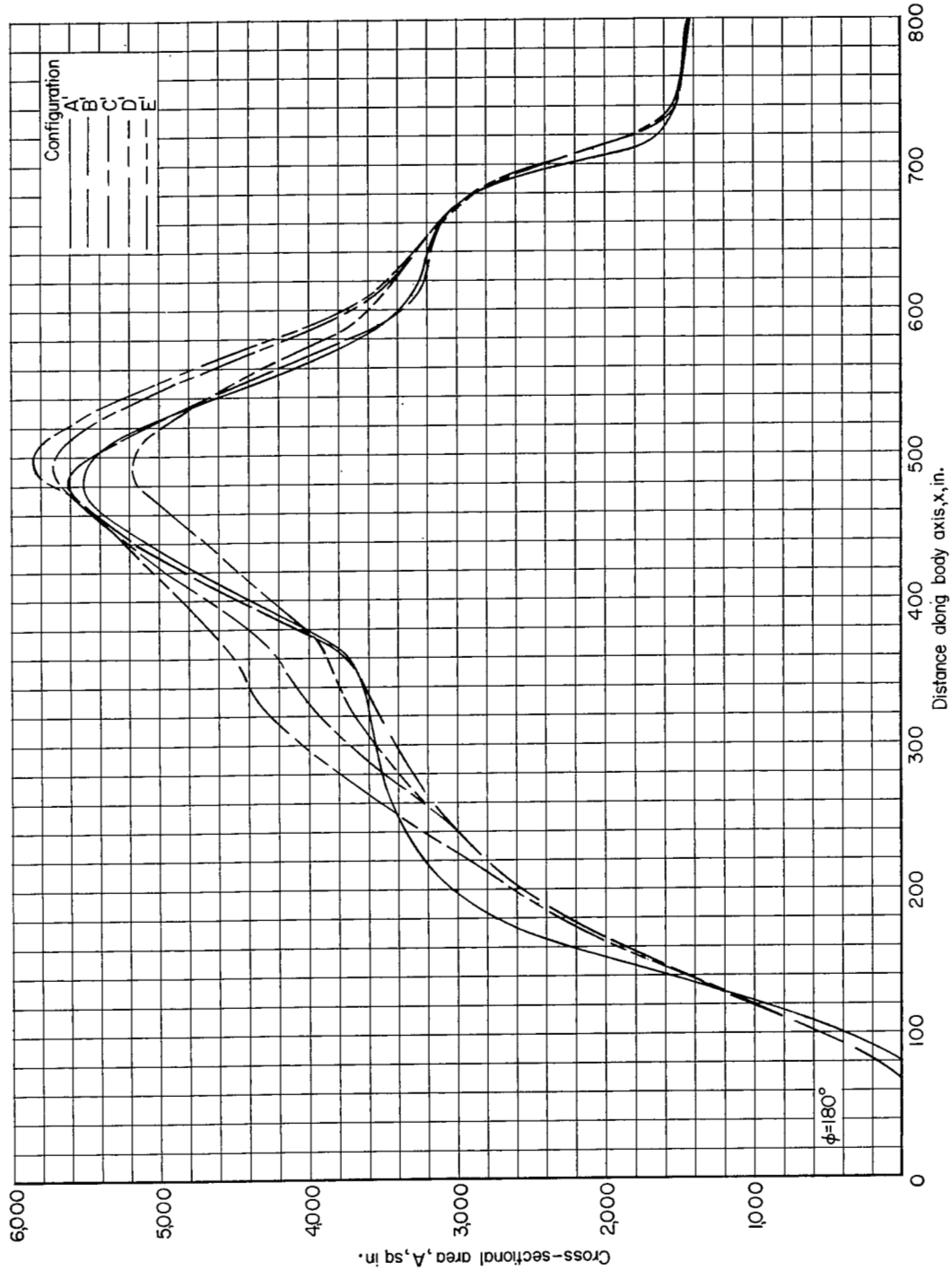

Figure 7.- Concluded.

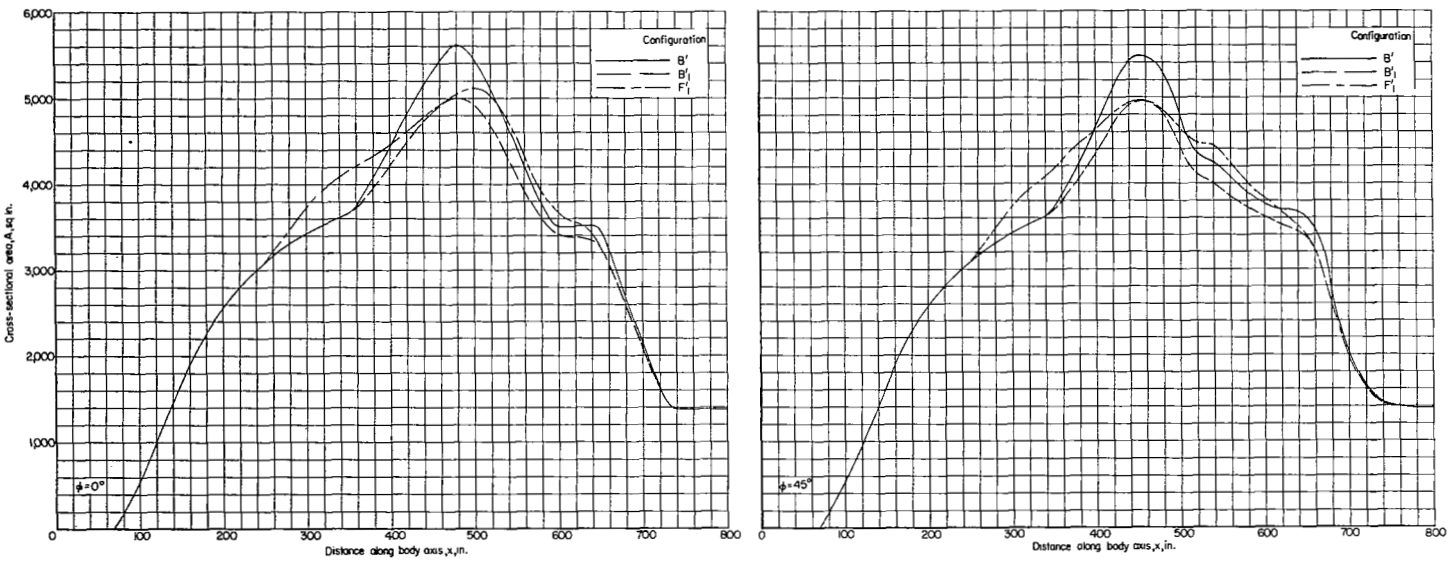

Figure 8.- Effect of empennage thickness on the area distributions. M = 1.2. (All dimensions are full scale.)

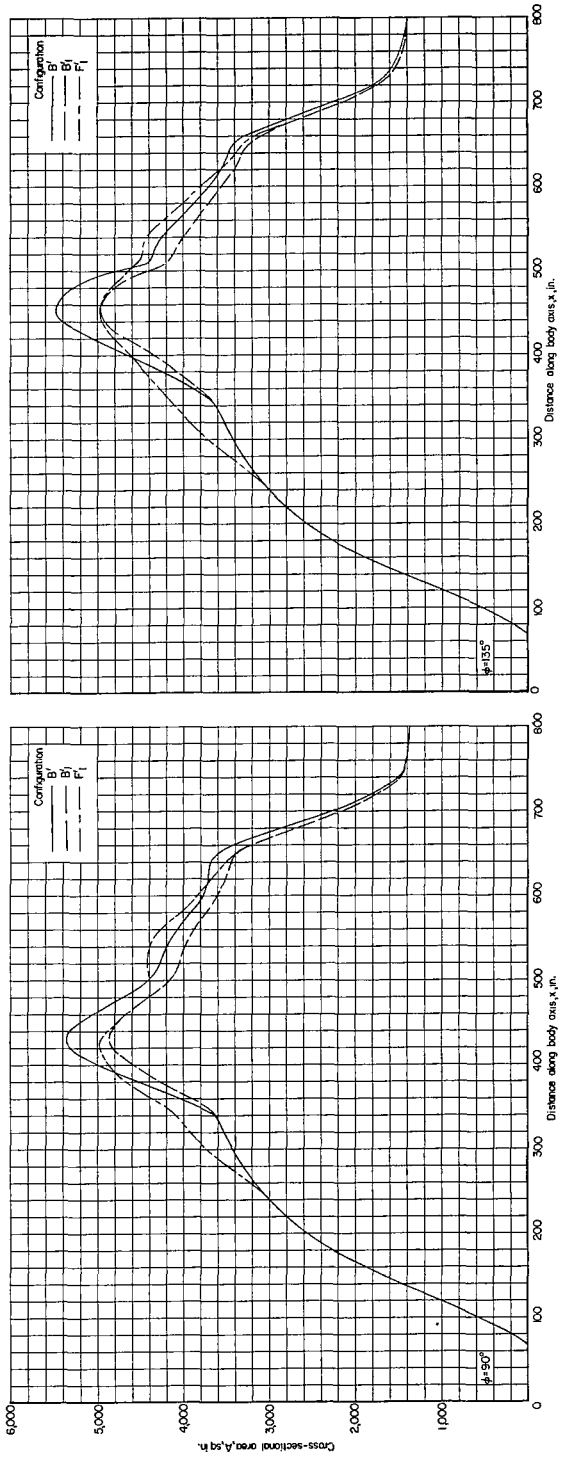

Figure 8.- Continued.

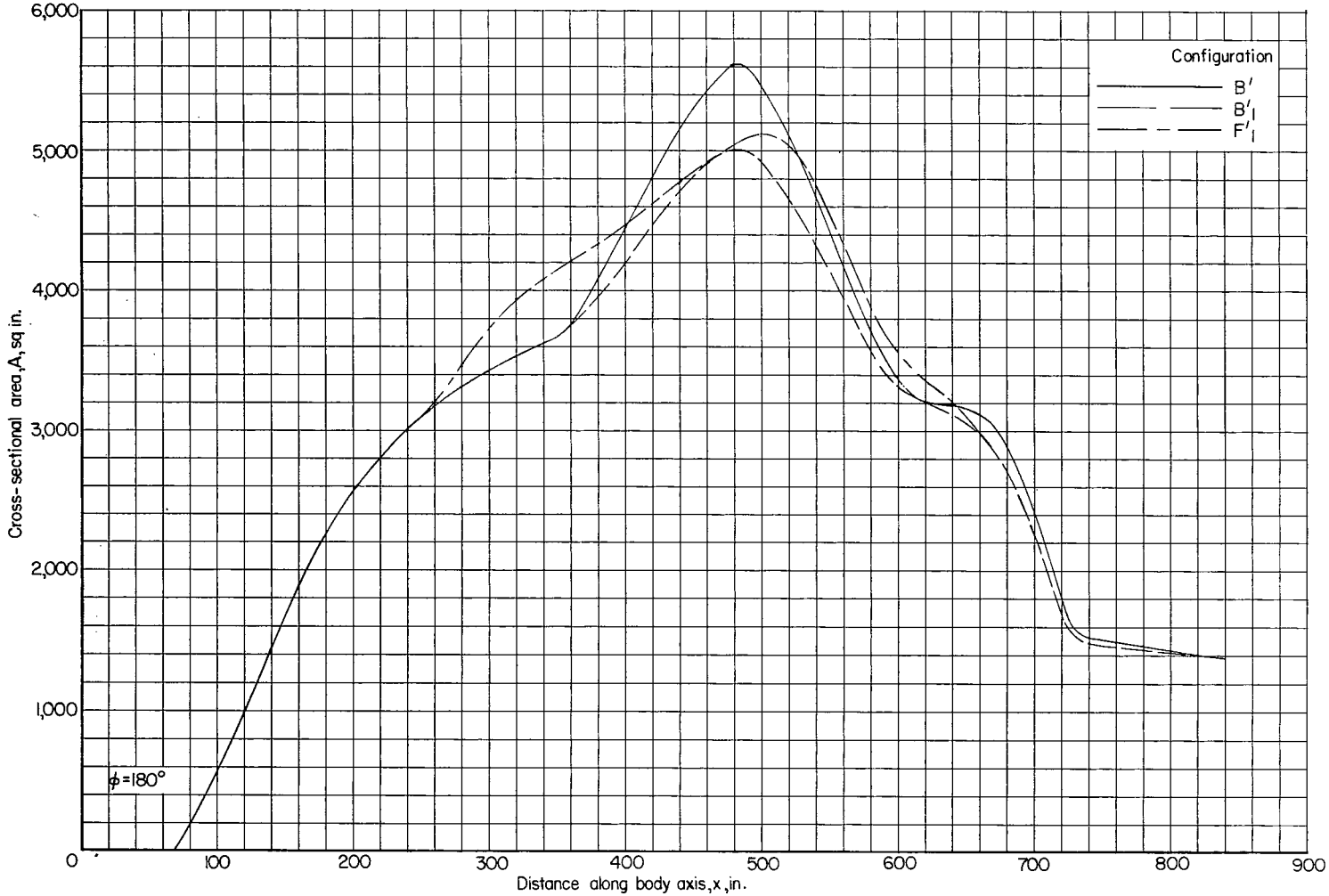

Figure 8.- Concluded.

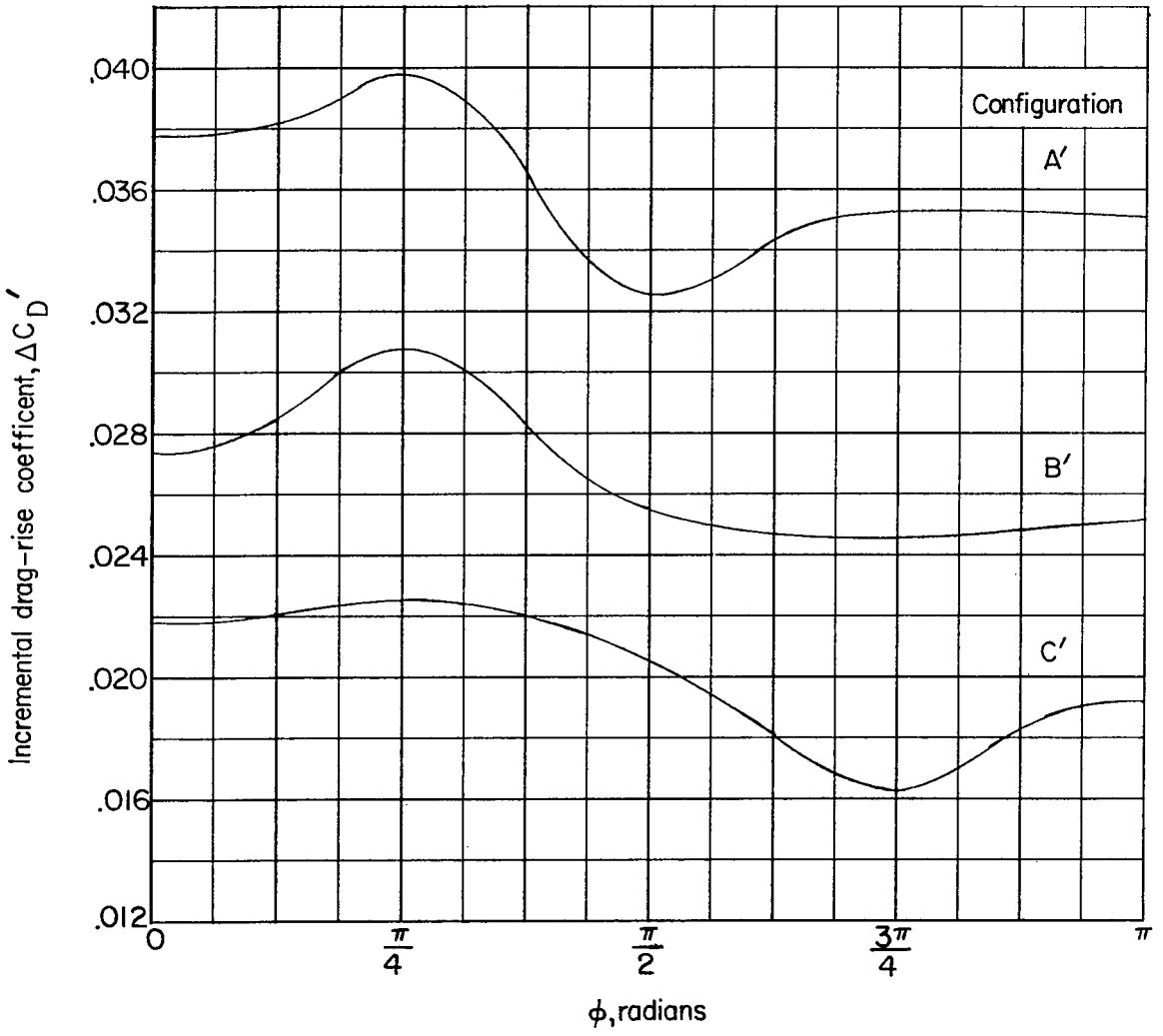

Figure 9.- Variation of incremental drag-rise coefficient with circumferential position. M = 1.2.

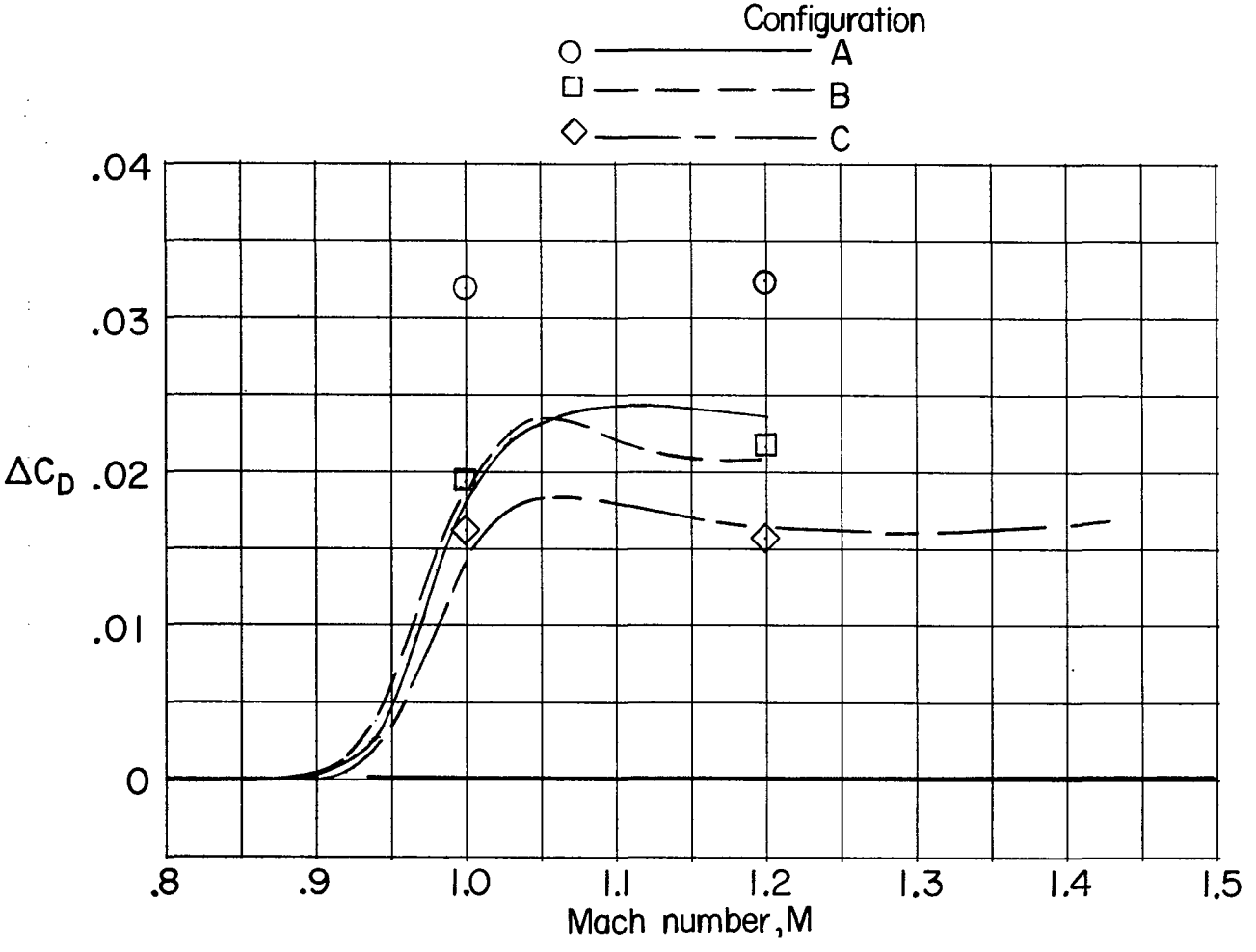

(a) Tail off; basic wing.

Figure 10.- Comparison of the calculated and experimental drag-rise coefficients with Mach number.

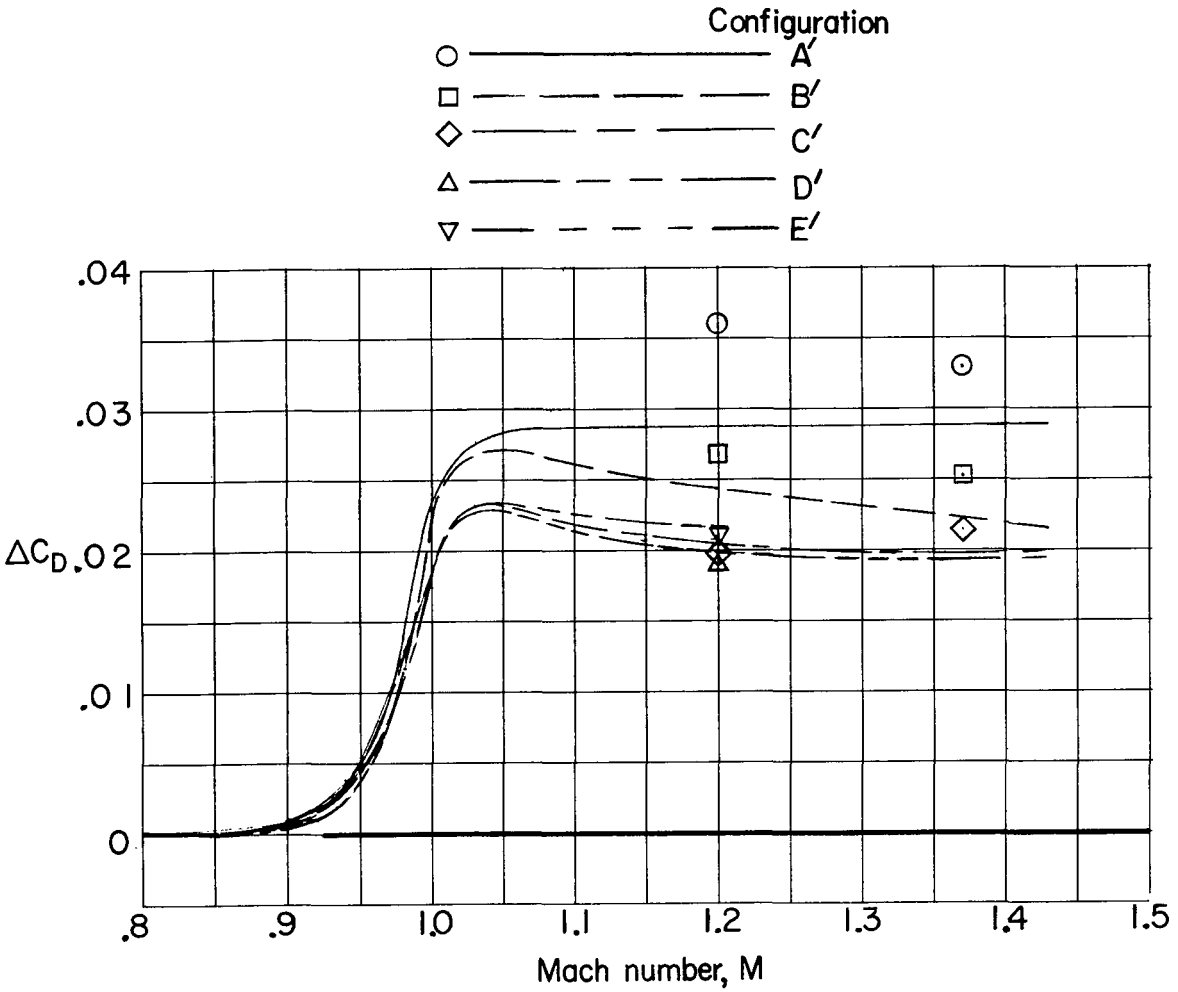

(b) Tail on; basic wing.

Figure 10.- Continued.

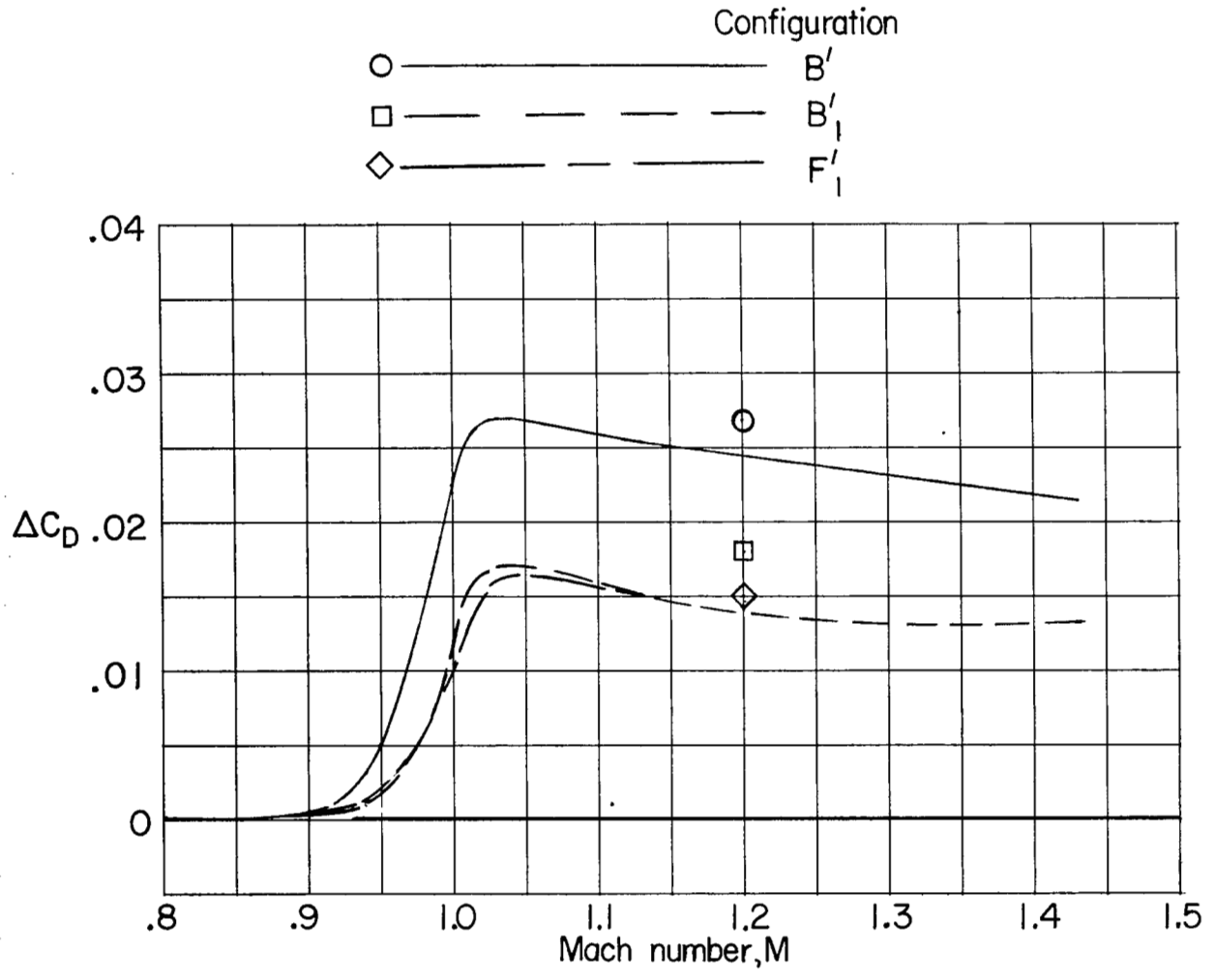

(c) Tail on; thin wing and thin tail.

Figure 10.- Concluded.

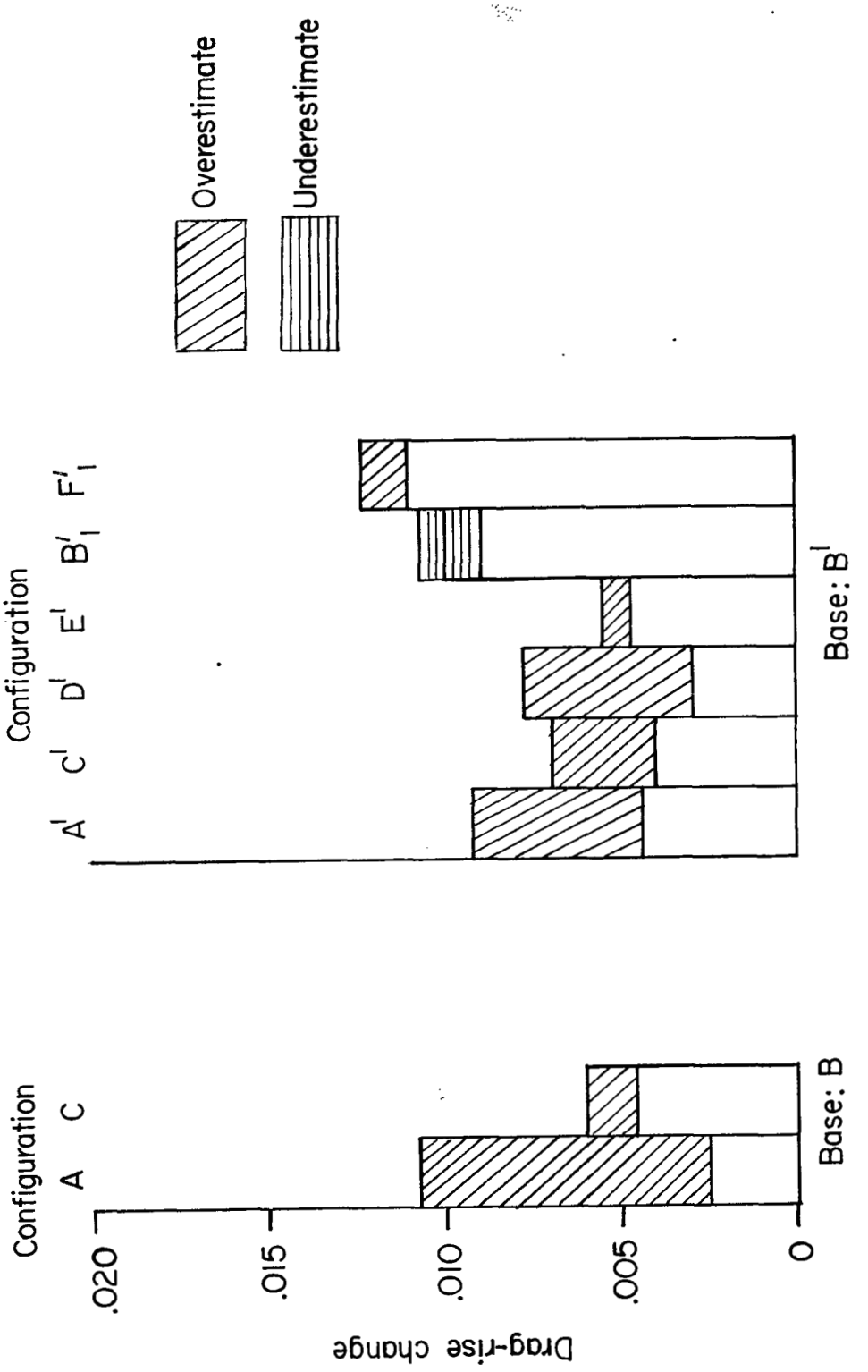

(a) Tails off. (b) Tails on.

Figure 11.- Comparison of estimated drag-rise increments. M = 1.20.